THE JOURNAL OF PHYSICAL CHEMISTRY A
A JOURNAL OF THE AMERICAN CHEMICAL SOCIETY

pubs.acs.org/JPCA

Article

Prototypical Allosterism in a Simple Ditopic Ligand: Gas-Phase Topologies of Cucurbit[n]uril·*n*-Alkylammonium Complexes Controlled by Binding in the Second Site

Jamir Shrestha, Savannah R. Porter, Caleb Tinsley, Andrew J. Arslanian, and David V. Dearden*

Cite This: *J. Phys. Chem. A* 2022, 126, 2950–2958

Read Online

ACCESS | Metrics & More | Article Recommendations | Supporting Information

ABSTRACT: We have employed mass spectrometry, ion mobility, and computational techniques to characterize complexes of *n*-alkylammonium ions with cucurbit[5]uril (CB[5]) and cucurbit[6]uril (CB[6]) ligands in the gas phase. Nonrotaxane structures are energetically preferred and experimentally observed for all CB[5] complexes. Pseudorotaxane structures are computationally favored and experimentally observed for [CB[6]·*n*-alkylammonium]$^+$ complexes, but the addition of a second cation (proton, alkali metal ion, another alkylammonium ion, or guanidinium) on the opposite rim of CB[6] causes sufficiently unfavorable steric interactions that *n*-pentylammonium and longer chains no longer remain threaded through the CB[6] cavity; nonrotaxane topologies are then favored. This provides a very simple example of negative allosteric interactions and molecular structure switching in these complexes.

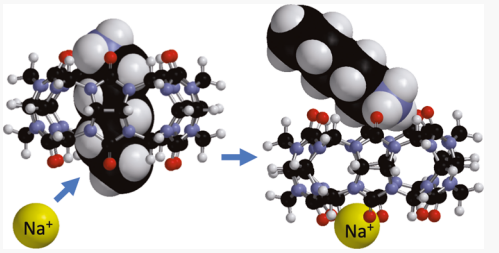

INTRODUCTION

Allosteric interactions[1−3] are a well-known phenomenon in biochemistry in which binding at a site remote from a protein's active site affects binding at the active site. These interactions can either enhance binding at other sites (cooperative binding), as in the binding of O_2 by hemoglobin,[4] or result in decreased binding (negative allosterism), as in the allosteric inhibition of HIV-RT by nevirapine and its analogues.[5,6] These kinds of interactions are important in such areas as regulation of metabolism and regulation of enzyme activity.[7]

Allosteric inhibition has been reported in proteins where the inhibitors bind to preformed binding sites. These inhibitors are usually ligands that bind with a protein to disrupt its overall native structure, affecting recognition in the active site.[8]

The binding of any ligand is generally based on the steric fit, structure, locality of the binding site, and binding affinity.[9] The allosteric capacity of a molecule depends on the capacity of changing these phenomena. Usually, organic complexes are used as allosteric promoters and inhibitors.[7] However, metal complexes have also been considered to cause allosteric interactions. Metal complexes including metals like Ga, Fe, Cu, Pd, and so forth have been successfully used as enzyme inhibitors.[10]

Cucurbit[n]urils (CB[n] hereafter, with n indicating the number of glycoluril units in these cyclic polymer molecules, Figure 1a) are very simple synthetic ditopic (2 binding sites) ligands, with the two well-defined identical binding sites a fixed, close distance apart.[1] This family of molecules, therefore, offers an opportunity to examine in detail how two proximate but separate binding sites interact through a simple type of allosterism,[2] with the possibility of seeing cooperative or anticooperative binding in a very simple system.[1,2] Previous gas-phase studies of CB[5] have observed anticooperative binding, as Coulomb repulsion due to binding a cation in one site weakens the binding of cations in the second site.[11] Although the portals and cavity of CB[5] are too small to accommodate threading of an alkyl chain, CB[6] and larger members of the family have been used as the ring component of rotaxanes (Figure 1b),[12−14] supramolecular structures consisting of a macrocyclic ring threaded onto a linear molecule. CB[6] and larger CB[n] use both sites in the binding of α,ω-*n*-alkyldiammonium cations as pseudorotaxanes (the bulky end groups usually used to prevent dethreading of

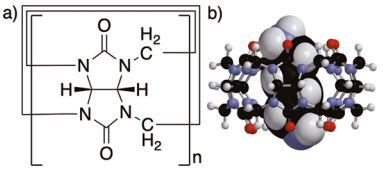

Figure 1. (a) Structure of cucurbit[*n*]uril. (b) Pseudorotaxane complex of 1,4-*n*-butanediammonium (space-filling) with cucurbit[6]-uril (ball and stick).

Received: March 10, 2022
Revised: April 22, 2022
Published: May 10, 2022

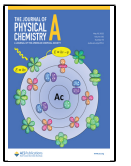

https://doi.org/10.1021/acs.jpca.2c01703
J. Phys. Chem. A 2022, 126, 2950−2958

threaded species in rotaxanes are not present), with strong preferences for alkyl chains of the appropriate length.[15−17]

In the gas phase, pseudorotaxanes with terminal or interior charged groups that are not intrinsically bulky can behave as if a bulky group were present because interactions between the charge and electronegative atoms in a host molecule can be strong enough to preclude facile dethreading.[15−17] In the case of CB[6] complexes with ammonium ions, the hydrogen bonding that occurs on the CB[6] rim is strong in the absence of a competing solvent, so ammonium-CB[6] binding effectively anchors the guest in the host.[15]

In this work we are interested in the intermediate case, *n*-alkylammonium guests that have a charged group on one end and a linear alkyl chain on the other. These ions cannot interact as strongly as the *α,ω-n*-alkyldiammonium cations because rather than having strong ionic hydrogen-bonding sites[18−24] on both ends, the alkyl tail can only support much weaker dispersion interactions; the enthalpic driving force for forming pseudorotaxanes is much weaker, and in fact, entropic considerations might tip the balance to favor having the *n*-alkyl tails outside the CB[6] cavity. Thus, one of the key questions here is whether or not CB[6] forms pseudorotaxanes with *n*-alkylammonium cations in the gas phase.

In addition, we investigate interactions between the two binding sites in these simple ditopic ligands, as a means of studying a simple type of allosteric interaction. Specifically, assuming that *n*-alkylammonium ions do form pseudorotaxanes with CB[6], how does binding a cation on the other rim affect the structure of the complex? Will it remain a pseudorotaxane, and if so, is there alkyl chain size dependence?

EXPERIMENTAL

Materials. CB[6] and *n*-alkylamines (n = 1−9, purity > 98%) were purchased from Sigma-Aldrich (St. Louis, MO). Both acetic acid (glacial) and HPLC-grade water were purchased from Fisher Scientific (Fair Lawn, NJ). Methanol was of LC−MS grade from Millipore Sigma (Burlington, MA). All materials were used without additional purification. Stock 200 μM CB[6] and 200 μM *n*-alkylamines were prepared by dissolving in 50:50 methanol/water. The stock solutions were mixed such that CB[6] was 20 μM and *n*-alkylamines were 40 μM in the final spray solution, which was also 0.5% acetic acid by volume.

Instrumentation. We used an Agilent model 6560 IMS-qToF instrument[25] for experimental collision cross-section (CCS) measurements. This instrument employed an Agilent-supplied nano-electrospray source, which was used for direct infusion electrospray and was equipped with a fragmentor ion optic that enabled in-source collision-induced dissociation. The instrument consisted of a uniform field ion mobility spectrometer (IMS) using nitrogen as the drift gas, placed between two ion funnel stages. The front ion funnel stage contained two sections where the ions were focused, trapped, and released into the drift tube. After the ions were separated in the drift tube, the ions were refocused into the collision cell, then transmitted to a quadrupole time-of-flight (qToF) mass spectrometer.

We used the stepped-field method[25] for CCS measurements, varying the overall voltage drop across the drift tube from 1000−1700 V in 8 increments and averaging data for 1 min at each field setting. CCS measurements in the IMS-qToF were calibrated against the m/z 922 ion of Agilent TuneMix. Drift times were measured at each field setting and were used to determine the collision cross sections in N_2 *via* application of the Mason−Schamp equation.[26]

Computational. Modeling in Spartan '18 (Wavefunction, Inc.; Irvine, CA, U.S.A.) began with a conformational search using the MMFF94 force field[27−31] supplied in the modeling package. Low energy structures found in the conformational search were subjected to single-point energy calculations using the M06-2X/6-31+G* method. Full geometry optimization using M06-2X/6-311G**//M06-2X/6-31G* was done on 3−5 of these lowest-energy isomers. The lowest-energy isomer at this level of theory was used for extracting the optimized geometry coordinates and ESP charges, which were employed in trajectory method CCS calculations in N_2 (with the N_2 quadrupole moment included and with partial charges on the ion) using IMoS 1.10c.[32]

RESULTS

Computed Energies. Computational modeling found minima for both nonrotaxane and pseudorotaxane structures of CB[5] and CB[6] complexes with *n*-alkylammonium guests. We calculated the difference in energy between the lowest-energy nonrotaxane and lowest energy pseudorotaxane structure for $[CB[n]\cdot RNH_3]^+$, $[CB[6]\cdot Na\cdot RNH_3]^{2+}$, and $[CB[6](RNH_3)_2]^{2+}$, with the results shown in Figure 2. All

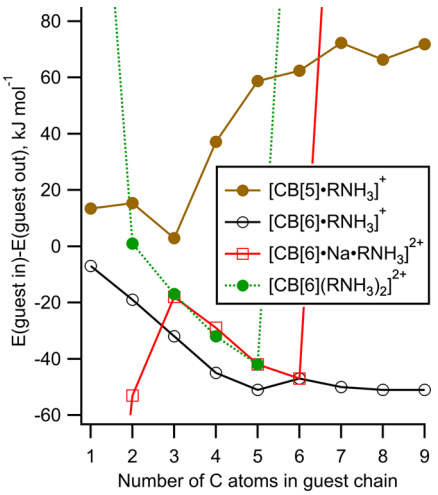

Figure 2. Difference in computed energy of pseudorotaxane ("guest in") and nonrotaxane ("guest out") structures, at the M06-2X/6-311G**//M06-2X/6-31G* level of theory, for CB[n] complexes involving *n*-alkylammonium guests as a function of the number of C atoms in the *n*-alkyl chain. Positive values indicate nonrotaxane structures are energetically favored, and negative values indicate pseudorotaxane structures are favored. Points not shown are off the scale.

the $[CB[5]\cdot RNH_3]^+$ complexes energetically favored nonrotaxane structures, whereas all the $[CB[6]\cdot RNH_3]^+$ complexes favored pseudorotaxanes. These preferences generally increase with increasing chain length. The nonrotaxane *versus* pseudorotaxane preferences for $[CB[n]\cdot Na\cdot RNH_3]^{2+}$ and $[CB[n](RNH_3)_2]^{2+}$ are more complex and are discussed in more detail below.

Experimental Observations. We observed both singly charged 1:1 and doubly charged 2:1 alkylammonium-CB[6] complexes, as well as doubly charged M^+ + alkylammonium + CB[6] complexes (where M is an alkali metal), with relative intensities strongly dependent on ion source conditions. The

https://doi.org/10.1021/acs.jpca.2c01703
J. Phys. Chem. A 2022, 126, 2950−2958

doubly charged complexes were observed under most conditions, whereas singly charged 1:1 complexes required more energetic source settings that favor collision-induced dissociation. Although our IM CCS measurements do yield absolute CCS values (please see the Supporting Information), in most cases we have chosen to report the results as ratios of the CCS value for the ion of interest to the CCS value for either $[CB[n]Na]^+$ (for singly charged ions) or $[CB[n]Na_2]^{2+}$ (for doubly charged ions), because by eliminating systematic deviations between experimentally measured and computed CCS values (likely due to imperfections in the modeling), this approach facilitates comparison with CCS ratios derived from the corresponding computed structures.

We note that the portals of CB[5] are considered too small to allow the formation of rotaxane structures, so structures in which the alkylammonium cations "perch" on the CB[5] rims are expected and, indeed, were the lowest-energy structures found by the calculations. These complexes, therefore, serve as controls to show trends in CCS values where the formation of rotaxanes does not occur.

In each case below, we will describe trends in the computed CCS values for CB[5] complexes as alkyl chain lengths increase, followed by a description of the experimentally measured results and a comparison between computed and experimental values. This same approach will then be followed for the corresponding CB[6] complexes, where, in contrast to CB[5], the portals of CB[6] are known from spectroscopic[12,13] and X-ray studies[14] to be large enough to facilitate rotaxane formation.

Singly Charged 1:1 Complexes of *n*-alkylammonium Ions with CB[n]. As expected, computational modeling found "perched," externally bound alkylammonium complexes to be the lowest-energy structures for each complex of CB[5] that was examined (Figure 2). Computed CCS values for these nonrotaxane complexes increase monotonically from 1−8 C atoms in the alkyl chain (Figure 3a), and drop a little for the nonylammonium complex as the alkyl chain begins to interact more strongly with the exterior of the host molecule, and perhaps reflecting the increasing difficulty of thoroughly exploring conformational space computationally for longer alkyl chain lengths.

Experimentally, all of the singly charged 1:1 alkylammonium complexes of CB[5] have single peaks in their arrival time distributions. The measured CCS ratios *versus* the CCS of $[CB[5]Na]^+$ increase monotonically with increasing alkyl chain length from 1−9 C atoms, with the rate of increase with chain length perhaps decreasing slightly for the longer chains (Figure 3a). The agreement between CCS ratios for the modeled structures and the experiment is good for 1−5 C atoms in the alkyl chain, but for longer chains, the ratios for the computed structures become increasingly smaller than the experimental values.

The portals of CB[6] are large enough that alkyl chains are observed to thread through them in crystallographic data for solid-phase complexes,[14] so we anticipated pseudorotaxane structures in the gas phase. We modeled both external alkyl tails (nonrotaxanes) and pseudorotaxane structures for each *n*-alkylammonium complexed with CB[6] (Figure 3b). As with the externally bound CB[5] complexes, the computed nonrotaxane structures of the 1:1 CB[6] complexes of *n*-alkylammonium ions increase monotonically in CCS as the alkyl chain length increases. In contrast, the computed pseudorotaxane structures for alkyl chains of 1−5 C atoms

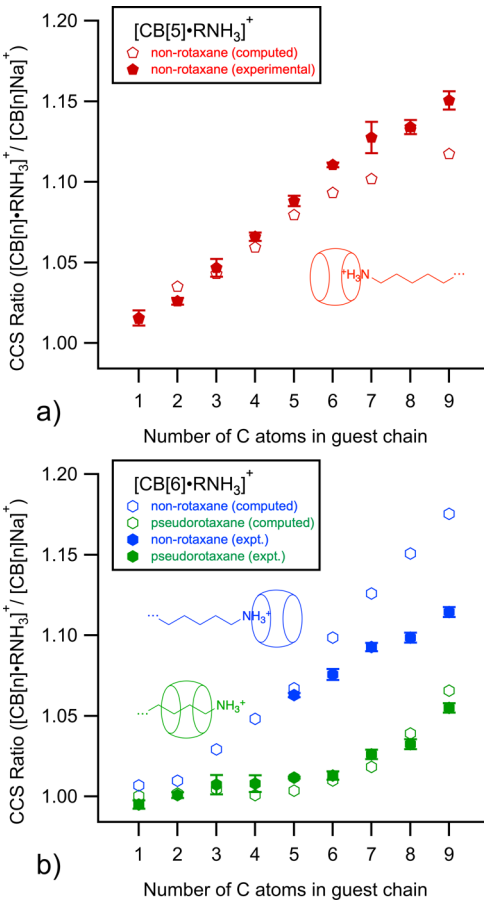

Figure 3. Collision cross sections relative to that of $[CB[n]Na]^+$ for singly charged complexes of (a) CB[5] or (b) CB[6] with *n*-alkylammonium ions with various alkyl chain lengths. Ratios from computed structures (M06-2X/6-31G*) are shown using open symbols, whereas those from experimental IMS measurements are shown using solid symbols. Inset cartoons are color-coded with the data to illustrate the structures.

have similar calculated CCS values, resulting primarily from the CB[6] host; the guest, inside the host, does not contribute appreciably to the CCS until the alkyl chain becomes long enough to protrude from the portal on the side opposite the ammonium group. This occurs for 6−9 C atoms in the *n*-alkylammonium chain.

In the experimental arrival time distributions for the CB[6] complexes of *n*-alkylammonium ions, single peaks were observed for chain lengths of 1−4 C atoms. The corresponding CCS ratios are near 1, indicating cross sections similar to that of $[CB[6]Na]^+$ and consistent with pseudorotaxane model structures that have the alkyl tail threaded inside the CB[6] cavity. This is particularly evident for propyl- and butylammonium cation guests, where there is a clear difference between computed CCS values for "tail in" and "tail out" structures.

For *n*-pentylammonium and longer guests, the experimental arrival time distributions had two peaks. The peaks at shorter arrival times for each complex, consistent with computed pseudorotaxane structures, were about twice as intense as those observed at longer arrival times, which were more consistent with computed nonrotaxane structures. The CCS ratios for the short-arrival-time structures, like those for the computed pseudorotaxane CB[6] complexes, increase for chain lengths greater than 5 or 6 C atoms, consistent with protrusion of the

https://doi.org/10.1021/acs.jpca.2c01703
J. Phys. Chem. A 2022, 126, 2950−2958

alkyl chain from the CB[6] portal opposite that where the ammonium group is bound. Like the nonrotaxane CB[5] complexes, the experimental CCS ratios for the CB[6] complexes observed at longer arrival times are increasingly smaller, as alkyl chain length increases, than those computed from trajectory method calculations.

Doubly Charged Complexes of M^+ and *n*-alkylammonium with CB[n]. Here we focus on M = Na, as these complexes are exemplary of those of other cations and were the most easily observed experimentally. Computational modeling of complexes with the $[CB[5]{\cdot}Na{\cdot}RNH_3]^{2+}$ stoichiometry found binding of the *n*-alkylammonium ions with the alkyl tails external to the CB[5] cavity as expected, and thus, yielded CCS ratios *versus* $[CB[5]Na_2]^{2+}$ (Figure 4a) that were all greater than 1, increasing monotonically with alkyl chain length up to 7 C atoms. The complex with *n*-octylammonium had a computed ratio a bit less than that of the *n*-heptylammonium complex, as the longer tail begins to wrap around the CB[5] host.

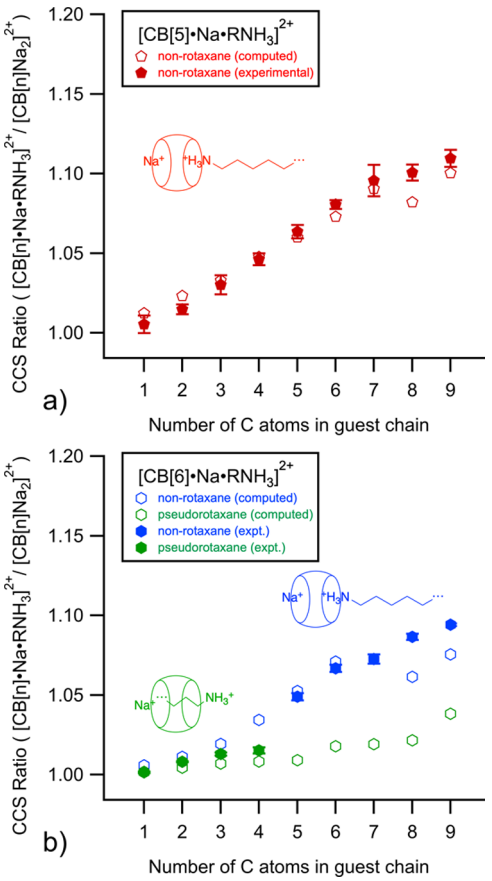

Figure 4. Collision cross sections relative to that of $[CB[n]Na_2]^{2+}$ for doubly charged complexes of (a) CB[5] or (b) CB[6] with Na^+ and *n*-alkylammonium ions with various alkyl chain lengths. Ratios from computed structures are shown using open symbols, whereas those from experimental IMS measurements are shown using solid symbols. Inset cartoons are color-coded to illustrate the structures and match the data.

Drift IMS measurements for $[CB[5]{\cdot}Na{\cdot}RNH_3]^{2+}$ found single peaks in the arrival time distributions for all complexes, with the corresponding CCS ratios relative to $[CB[5]Na_2]^{2+}$ all greater than 1, increasing monotonically with the *n*-alkylammonium chain length for all observed complexes. Agreement between the computationally modeled and experimentally observed ratios is good, suggesting that all of the observed $[CB[5]{\cdot}Na{\cdot}RNH_3]^{2+}$ complexes have nonrotaxane structures with alkyl tails external to the CB[5] cavity.

We modeled both nonrotaxane and pseudorotaxane structures for $[CB[6]{\cdot}Na{\cdot}RNH_3]^{2+}$, with CCS ratio results given in Figure 4b. The nonrotaxane structures have CCS ratios *versus* $[CB[6]Na_2]^{2+}$ that are all greater than 1 and increase monotonically with alkyl chain length as expected, with some scatter for the longest alkyl tails as chain wrapping occurs and comprehensive modeling becomes more difficult. The pseudorotaxane structures for complexes with 1−5 C atoms in the alkyl tails all have similar computed CCS ratios slightly greater than 1, again reflecting the internal binding of the alkyl tails. For 6 C atoms and longer, the alkyl tails are too long to fit within the CB[6] cavity and begin to push out, by disrupting either the hydrogen bonding of the ammonium group with the CB[6] rim O atoms and/or the interaction of the Na^+ ion with the opposite rim.

In contrast to our observations of the singly charged complexes of alkylammonium cations with CB[6]), where we saw multiple peaks in the arrival time distribution for complexes of *n*-pentylammonium and longer *n*-alkylammonium ions, when Na^+ is also present, resulting in a doubly charged complex, only single peaks are observed in the arrival time distributions for each complex. As seen in Figure 4b, complexes with *n*-butylammonium and shorter-chain *n*-alkylammonium ions all have similar, relatively small collision cross sections (less than 2% larger than the CCS of $[CB[6]Na_2]^{2+}$). These are consistent with the computed CCS ratios for pseudorotaxane structures. The cross section increases by about 10 Å^2 (to about 5% larger than that of $[CB[6]Na_2]^{2+}$) when *n*-butylammonium is replaced by *n*-pentylammonium. All longer-chain complexes follow this same trend of much larger CCS, with CCS increasing with chain length. For *n*-pentylammonium and longer chains, the CCS ratios are more consistent with those for computed nonrotaxane structures. Also in qualitative but not quantitative agreement, the computed energies (Figure 2) suggest pseudorotaxane structures for the Na^+-containing species are favored for chains as long as 6 carbon atoms, whereas for longer chains the nonrotaxane structures are very strongly favored.

This switch from pseudorotaxane to nonrotaxane topology with increasing alkyl chain length when Na^+ is bound to CB[6] is also observed when Na^+ is replaced by H^+, Li^+, K^+, Cs^+, NH_4^+, or guanidinium (see Supporting Information). For each of these cations, a similarly significant increase in collision cross section occurs when *n*-butylammonium is replaced by *n*-pentylammonium or a longer *n*-alkylammonium. This suggests that in all the $[CB[6]{\cdot}M{\cdot}RNH_3]^{2+}$ complexes we have observed in the gas phase, for R = *n*-butyl and shorter chains the complexes are pseudorotaxanes, whereas, for R = *n*-pentyl and longer chains, the presence of M^+ causes a nonrotaxane structure to be favored.

A small but interesting difference is observed when $M^+ = H^+$ or guanidinium (Supporting Information, Table S1 and Figure S1). As with the other capping cations, complexes of *n*-alkylammonium ions having *n*-butyl or shorter chains gave single peaks in the arrival time distributions, consistent with pseudorotaxane structures. For $M^+ = H^+$, two peaks are seen in the distribution for $[CB[6]{\cdot}H{\cdot}n\text{-pentylammonium}]^{2+}$. Longer *n*-alkyl chains yielded only the longer-arrival-time peaks,

https://doi.org/10.1021/acs.jpca.2c01703
J. Phys. Chem. A 2022, 126, 2950−2958

consistent with nonrotaxane structures. Similarly, for M^+ = guanidinium, two peaks are observed in the arrival time distributions for the complexes involving *n*-pentyl- and *n*-hexylammonium; longer *n*-alkyl chains resulted in only the longer-arrival-time peaks. Possible explanations are discussed below.

Doubly Charged $[CB[n](RNH_3)_2]^{2+}$ Complexes. We also examined doubly charged complexes with stoichiometry $[CB[n](RNH_3)_2]^{2+}$. These complexes have more topological possibilities, as they may have structures with both *n*-alkyl tails inside the CB[n] ("in−in"), structures with one tail in and one out ("in−out"), or structures with both tails out ("out−out").

Based on the results for the singly charged $[CB[n]\cdot RNH_3]^+$ complexes, we would expect all $[CB[5](RNH_3)_2]^{2+}$ complexes to be out−out, because the CB[5] portal is too small to easily accommodate an alkyl chain. Computationally, all of the $[CB[5](RNH_3)_2]^{2+}$ complexes were modeled as out−out structures with both *n*-alkyl tails exterior to the CB[5] ligand. Their CCS ratios relative to that of $[CB[5]Na_2]^{2+}$ (Figure 5a) increase with the increasing chain length up through *n*-hexylammonium, and for longer chains, while remaining large, show more scatter due to wrapping of the alkyl chains around the CB[5] and perhaps increasing difficulty in properly exploring the conformational space, the same as was seen for $[CB[5]\cdot RNH_3]^+$ and $[CB[5]\cdot Na\cdot RNH_3]^{2+}$ complexes.

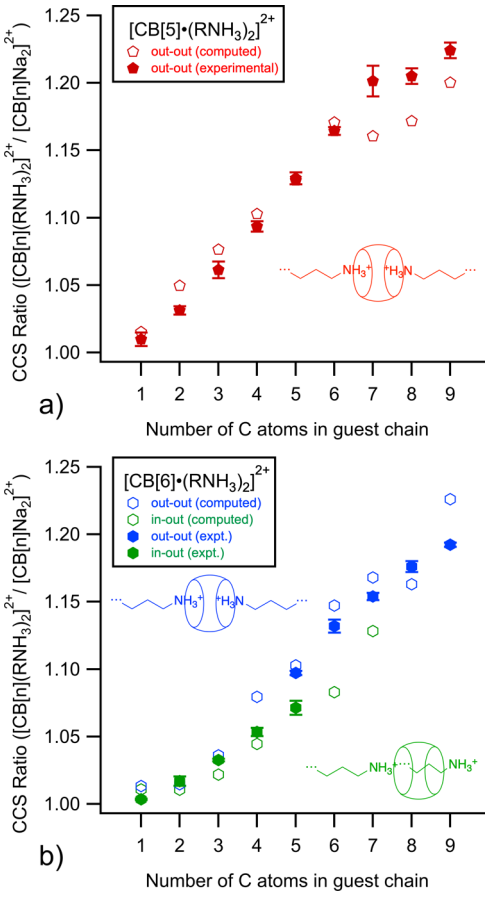

Figure 5. Collision cross sections relative to that of $[CB[n]Na_2]^{2+}$ for doubly charged complexes of (a) CB[5] or (b) CB[6] with 2 identical *n*-alkylammonium ions with various alkyl chain lengths. Ratios from computed structures are shown using open symbols, whereas those from experimental IMS measurements are shown using solid symbols. Inset cartoons are color-coded to illustrate the structures and match the data.

Experimental drift IMS measurements for $[CB[5](RNH_3)_2]^{2+}$ complexes gave single peaks in their arrival time distributions, and CCS ratios relative to the CCS of $[CB[5]Na_2]^{2+}$ (Figure 5a) increase with the increasing *n*-alkylammonium chain length. These observations are in good qualitative agreement with the computed results for out−out complexes.

In computational studies of $[CB[6](RNH_3)_2]^{2+}$, in−in complexes were found only for R = *n*-propyl and shorter and were not the lowest-energy structures in any case. The in−out and out−out complexes are similar in cross section for the smallest *n*-alkylammonium guests, becoming appreciably different only for 3 C atoms in the chain and longer (Figure 5b), but unsurprisingly, the CCS ratios for a given stoichiometry increase in the order in−in < in−out < out−out for all examined chain lengths. The computed CCS ratios relative to that of $[CB[6]Na_2]^{2+}$ (Figure 5b) increase with chain length up to *n*-heptylammonium, once again exhibiting some scatter for longer chains. No minimum was found for in−out structures involving *n*-nonylammonium. Energetically (Figure 2), the out−out structure is strongly favored for methylammonium and slightly favored for ethylammonium. In−out structures are favored for *n*-propyl-, *n*-butyl-, and *n*-pentylammonium, whereas out−out structures are strongly favored for all longer *n*-alkylammonium chains.

Experimentally, single peaks were observed in the arrival time distributions for all $[CB[6](RNH_3)_2]^{2+}$ species except that for R = *n*-pentyl, where two peaks were seen (Figure 5b). The CCS ratio for the smaller of these follows the smooth trend of the methylammonium—*n*-butylammonium complexes, whereas the CCS ratio of the larger *n*-pentylammonium complex jumps about 2% and begins a new smooth trend for the complexes of the longer *n*-alkylammonium ions. The experimental CCS ratios for the smaller $[CB[6](n\text{-pentylammonium})_2]^{2+}$ complex and the complexes of the shorter *n*-alkylammonium ions are in good agreement with the theoretical CCS ratios for the computed in−out structures. For the larger complex of *n*-pentylammonium and the longer *n*-alkylammonium ions, the experimental values are in better agreement with theory-derived out−out structures.

Doubly Charged $[CB[6](RNH_3)(R'NH_3)]^{2+}$ Complexes. Finally, we observed complexes with the $[CB[6](RNH_3)(R'NH_3)]^{2+}$ stoichiometry (i.e., complexes with two different *n*-alkylammonium ions bound to CB[6]). These complexes were examined computationally using molecular mechanics techniques, but because of the many low-energy conformers involved, they were not studied with the higher-level computational methods that yield more accurate energies and structures. Instead, we focus on experimental drift IMS results for these systems. Collision cross section ratios measured for these systems *versus* that of $[CB[6]Na_2]^{2+}$ are plotted in Figure 6 as a function of the number of C atoms in the second guest, while the first guest is held constant in each of the data sets shown.

In general, the complexes increase in cross section as the length of the alkyl chains R and R′ increase. All the data except those for the *n*-butylammonium complexes show a significant increase in the relative cross section between 4 and 5 C atoms in the R′ guest.

Energy-Resolved Collision-Induced Dissociation. We performed energy-resolved collision-induced dissociation

https://doi.org/10.1021/acs.jpca.2c01703
J. Phys. Chem. A 2022, 126, 2950−2958

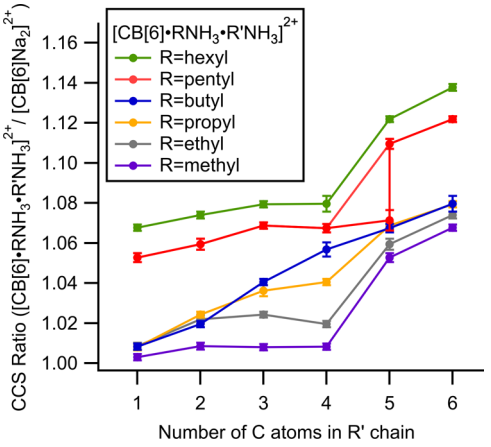

Figure 6. Collision cross sections relative to that of $[CB[6]Na_2]^{2+}$ for doubly charged complexes of CB[6] with 2 mixed *n*-alkylammonium ions with various alkyl chain lengths.

(CID) experiments on ions exiting the ion mobility stage of our IMS-ToF instrument, in an effort to determine whether there is a strong binding preference for particular *n*-alkylammonium ions in the CB[n] complexes, akin to what has previously been observed for *α,ω*-*n*-alkyldiammonium guests in CB[6].[16,17] In Figure 7, we show results for energy-resolved CID of five $[CB[5](RNH_3)(R'NH_3)]^{2+}$ complexes and the corresponding five $[CB[6](RNH_3)(R'NH_3)]^{2+}$ complexes, plotted as the survival yield, the fraction of intact precursor remaining. Generally, these dissociations occur with at least a small preference for loss of the longer *n*-alkylammonium ion. All of the CB[5] complexes dissociate at similar energies (50% of the precursor dissociating around 0.34 ± 0.01 eV), on average perhaps slightly lower than the energies required to dissociate the CB[6] complexes (average 50% dissociation at 0.36 ± 0.02 eV, excluding the anomalously high value for [CB[6](*n*-hexylammonium)(*n*-octylammonium)]$^{2+}$ that was observed with poor signal-to-noise), as expected due to the greater polarizability and larger number of internal degrees of freedom of the larger cucurbituril host. Interestingly, both [CB[6](*n*-propylammonium)(*n*-hexylammonium)]$^{2+}$ and [CB[6](*n*-butylammonium)(*n*-pentylammonium)]$^{2+}$ dissociate around 0.35 eV, similar to the CB[5] complexes, whereas the other CB[6] complexes appear to dissociate at slightly higher energies. In any event, the spread in dissociation energies is small enough that no clear binding preferences are evident.

DISCUSSION

Evidence for Pseudorotaxane Structures in Gas Phase Complexes of CB[6] with *n*-alkylammonium Ions. Computational data, in combination with CCS measurements, provide good evidence for [CB[6](*n*-alkylammonium)]$^{+}$ pseudorotaxane structures in the gas phase. The computational results shown in Figure 2 indicate an energetic preference for pseudorotaxane structures over nonrotaxanes that increases with increasing chain length up to about 50 kJ mol^{-1} for 4−5 C atoms in the chain and longer. This reflects increasing dispersion interactions between the alkyl chain and the CB[6] interior that top out when the alkyl chain is the same length as the length of the CB[6] cavity. The collision-induced dissociation data shown in Figure 7 also suggest similar dissociation energies for all CB[5] complexes and CB[6] complexes, where a longer *n*-alkylammonium cation is bound externally. Complexes with the *n*-butyl tail dispersively held inside the CB[6] cavity appear to dissociate at somewhat higher energies. However, we have no simple explanation for the significantly higher dissociation energies observed for the CB[6](*n*-hexylammonium)(*n*-octylammonium)]$^{2+}$ complex. While this is the largest complex examined, and therefore might be expected to exhibit the largest influence of energy partitioning into internal degrees of freedom with a concomitant decrease in dissociation rates,[33−36] the shift in dissociation energies seems too large to attribute to kinetic shifts[37] and may simply be due to poor signal-to-noise in those measurements.

CCS measurements also support these conclusions. However, control experiments measuring CCS ratios for CB[5] complexes, which should be nonrotaxanes, were in good agreement with computed nonrotaxane structures, experimental CCS ratios for the more abundant, shorter

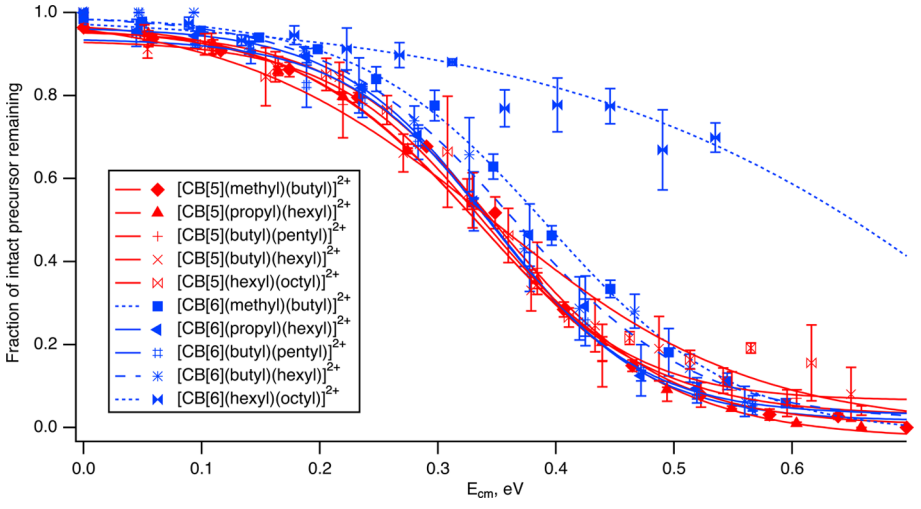

Figure 7. Precursor ion survival curves for selected complexes of CB[5] and CB[6] with two *n*-alkylammonium cations with different chain lengths, subjected to collision-induced dissociation at the indicated center-of-mass energies (E_{cm}) in N_2. Error bars are standard deviations from 3 repeated experiments; lines are sigmoidal fits to each data set.

https://doi.org/10.1021/acs.jpca.2c01703
J. Phys. Chem. A 2022, 126, 2950−2958

arrival time CB[6] complexes are in good agreement with those for computed pseudorotaxane structures (Figure 3). These values are significantly smaller than those for the corresponding computed nonrotaxane structures. Similar arguments (based primarily on experimental CCS measurements) can be made for $[CB[6]{\cdot}M{\cdot}RNH_3]^{2+}$ (Figure 4) and $[CB[6](RNH_3)_2]^{2+}$ (Figures 5 and 6) complexes with chain lengths less than 5 C atoms. In each of these cases, complexes involving *n*-alkyl chains shorter than *n*-pentyl have CCS values similar to those of the model rotaxane structures and smaller than the trend expected for the complexes of the longer *n*-alkylammonium ions.

Interactions between the two CB[6] binding sites for cations cause structural changes in *n*-alkylammonium complexes of CB[6]. The complexes examined here provide one of the simplest examples of allosteric interactions between two binding sites. When an additional ion is bound on the CB[6] portal opposite to where an *n*-alkylammonium cation is bound, additional steric requirements are introduced into the resulting complex, effectively closing the CB[6] portal where the additional cation is bound and inducing an allosteric change in the binding of the *n*-alkylammonium ion. This is evident in the switch from a preference for pseudorotaxane structures (for all *n*-alkyl chain lengths examined) when a second cation is not bound to a preference for nonrotaxane structures in the presence of a second cation (alkali metal ions and alkylammonium ions appear to similarly cause this switching in preference) for *n*-pentylammonium and longer chains (Figures 4 and 5). These experimental results are consistent with computed relative energies for complexes with up to 4 C atoms in the *n*-alkyl chain (pseudorotaxane preferred) and for greater than 6 C atoms in the *n*-alkyl chain (nonrotaxane preferred) but are not consistent with the calculated energetic preferences for *n*-pentylammonium or *n*-hexylammonium complexes, which computationally have pseudorotaxane preferences, but experiments suggest them to be nonrotaxanes. The reasons for this disagreement between theory and experiment are not clear; perhaps a higher-level theory is needed to describe the system accurately.

In this context, the two small exceptions to the general trend for $[CB[6]{\cdot}M{\cdot}RNH_3]^{2+}$ complexes, when $M^+ = H^+$ or M^+ = guanidinium, are interesting. In the case of a proton bound on the opposite rim, the amount of steric hindrance is relatively small because the proton is too small to simultaneously interact with all of the carbonyl oxygen atoms. This allows both pseudorotaxane and nonrotaxane isomers of the *n*-pentylammonium complex to be observed. Guanidinium is only weakly bound to CB[6][38] (see also Supporting Information Figure S3) and apparently, this "looser" fit makes it possible to observe both pseudorotaxane and nonrotaxane forms of the *n*-pentyl- and *n*-hexylammonium complexes.

The observed patterns in the data shown in Figure 6 (two *n*-alkylammonium cations bound to CB[6]) are especially illuminating. These patterns can be understood in terms of a preference for the longer chain up to *n*-butylammonium to be inside the CB[6] cavity, thus maximizing favorable dispersion interactions. Chains longer than 4 C atoms preferentially bind outside in these complexes because otherwise, their length would cause them to suffer unfavorable steric interactions with the ammonium group bound on the opposite rim. For example, the complexes with R = *n*-propyl- or *n*-butylammonium (Figure 6) are similar in cross section in most cases because both *n*-propyl and *n*-butyl are inside the CB[6] cavity and do not contribute to the CCS; the CCS is determined primarily by the CB[6] ligand and the other *n*-alkylammonium. This other guest is either shorter than *n*-propyl or *n*-butyl and thus bound externally because it is energetically more favorable for *n*-propyl or *n*-butyl to be inside or is too long for the CB[6] cavity such that it suffers unfavorable steric interactions and is thus bound externally. The $[CB[6](n\text{-butylammonium})_2]^{2+}$ CCS is larger than that of the $[CB[6](n\text{-propylammonium})(n\text{-butylammonium})]^{2+}$ complex because in the former one *n*-butyl tail is out, whereas in the latter the smaller *n*-propyl tail is out. Similarly, large increases in CCS in going from $[CB[6](n\text{-butylammonium})(n\text{-pentylammonium})]^{2+}$ to $[CB[6](n\text{-pentylammonium})_2]^{2+}$ and in going from $[CB[6](n\text{-butylammonium})(n\text{-hexylammonium})]^{2+}$ to $[CB[6](n\text{-pentylammonium})(n\text{-hexylammonium})]^{2+}$ suggest that the latter of each of these pairs of complexes has both alkyl tails outside; if one were inside, it would be long enough to interfere with binding of the 2nd alkylammonium cation, so the in−out topology is not preferred.

CONCLUSIONS

When *n*-alkylammonium ions bind with CB[6], pseudorotaxanes are preferentially formed because of favorable dispersion interactions between the *n*-alkyl tail of the guest and the interior of the host. However, these favorable interactions can easily be disrupted by binding a second cation on the opposite portal of the CB[6] host. This changes the shape of the binding site from one resembling an open tube to a closed, cup-like geometry, into which long *n*-alkyl chains no longer fit. The relatively strong electrostatic interactions between most of the second cations examined and the CB[6] portal O atoms are sufficient to cause this geometric change and displacement of *n*-alkyl tails longer than *n*-butyl. These simple, prototypical allosteric interactions can be used to understand and design molecular switches based on changes in the binding site topology upon binding a second guest cation.

ASSOCIATED CONTENT

Supporting Information

The Supporting Information is available free of charge at https://pubs.acs.org/doi/10.1021/acs.jpca.2c01703.

Table of experimentally measured collision cross sections in N_2 drift gas; variation in experimentally measured collision cross sections of $[CB[6]{\cdot}M{\cdot}n\text{-alkylammonium}]^{2+}$ for various M^+ cations; typical arrival time distribution heat map; and $[CB[6]M_2]^{2+}$ collision-induced dissociation experiments (PDF)

AUTHOR INFORMATION

Corresponding Author

David V. Dearden − *Department of Chemistry and Biochemistry, Brigham Young University, Provo, Utah 84602-1030, United States;* orcid.org/0000-0003-0899-7776; Phone: 801-422-2355; Email: dvd@chem.byu.edu

Authors

Jamir Shrestha − *Department of Chemistry and Biochemistry, Brigham Young University, Provo, Utah 84602-1030, United States*

Savannah R. Porter − *Department of Chemistry and Biochemistry, Brigham Young University, Provo, Utah 84602-1030, United States*

Caleb Tinsley − *Department of Chemistry and Biochemistry, Brigham Young University, Provo, Utah 84602-1030, United States*

Andrew J. Arslanian − *Department of Chemistry and Biochemistry, Brigham Young University, Provo, Utah 84602-1030, United States*

Complete contact information is available at: https://pubs.acs.org/10.1021/acs.jpca.2c01703

Author Contributions

The manuscript was written through the contributions of all authors.

Notes

The authors declare no competing financial interest.

■ ACKNOWLEDGMENTS

We are grateful to the U. S. National Science Foundation for supporting this work (CHE-1904838), the BYU College of Physical and Mathematical Sciences for funds to support the undergraduate research, and the BYU Office of Research Computing for computational resources.

■ REFERENCES

(1) Isaacs, L. Cucurbit[n]urils: From Mechanism to Structure and Function. *Chem. Commun.* **2009**, 619−629.

(2) Lemaur, V.; Carroy, G.; Poussigue, F.; Chirot, F.; De Winter, J.; Isaacs, L.; Dugourd, P.; Cornil, J.; Gerbaux, P. Homotropic Allosterism: In-Depth Structural Analysis of the Gas-Phase Non-covalent Complexes Associating a Double-Cavity Cucurbit[n]uril-Type Host and Size-Selected Protonated Amino Compounds. *ChemPlusChem* **2013**, *78*, 959−969.

(3) Hess, V. L.; Szabo, A. Ligand Binding to Macromolecules: Allosteric and Sequential Models of Cooperativity. *J. Chem. Educ.* **1979**, *56*, 289−293.

(4) Perutz, M. F. Hemoglobin Structure and Respiratory Transport. *Sci. Am.* **1978**, *239*, 92−125.

(5) Esnouf, R.; Ren, J.; Ross, C.; Jones, Y.; Stammers, D.; Stuart, D. Mechanism of Inhibition of HIV-1 Reverse Transcriptase by Non-Nucleoside Inhibitors. *Nat. Struct. Biol.* **1995**, *2*, 303−308.

(6) Ren, J.; Nichols, C.; Bird, L.; Chamberlain, P.; Weaver, K.; Short, S.; Stuart, D. I.; Stammers, D. K. Structural Mechanisms of Drug Resistance for Mutations at Codons 181 and 188 in HIV-1 Reverse Transcriptase and the Improved Resilience of Second Generation Non-Nucleoside Inhibitors. *J. Mol. Biol.* **2001**, *312*, 795−805.

(7) Nelson, D. L.; Cox, M. M. *Lehninger Principles of Biochemistry*; 7th ed.; W. H. Freeman: New York, 2017.

(8) Horn, J. R.; Shoichet, B. K. Allosteric Inhibition through Core Disruption. *J. Mol. Biol.* **2004**, *336*, 1283−1291.

(9) Miller, D. W.; Dill, K. A. Ligand Binding to Proteins: The Binding Landscape Model. *Protein Sci.* **1997**, *6*, 2166−2179.

(10) Louie, A. Y.; Meade, T. J. Metal Complexes as Enzyme Inhibitors. *Chem. Rev.* **1999**, *99*, 2711−2734.

(11) Mortensen, D. N.; Dearden, D. V. Influence of Charge Repulsion on Binding Strengths: Experimental and Computational Characterization of Mixed Alkali Metal Complexes of Decamethylcucurbit[5]uril in the Gas Phase. *Chem. Commun.* **2011**, *47*, 6081−6083.

(12) Mock, W. L.; Shih, N. Y. Structure and Selectivity in Host Guest Complexes of Cucurbituril. *J. Org. Chem.* **1986**, *51*, 4440−4446.

(13) Buschmann, H.-J.; Wego, A.; Schollmeyer, E.; Döpp, D. Synthesis of Cucurbituril-Spermine-[2]Rotaxanes of the Amide-Type. *Supramol. Chem.* **2000**, *11*, 225−231.

(14) Kim, K. Mechanically Interlocked Molecules Incorporating Cucurbituril and Their Supramolecular Assemblies. *Chem. Soc. Rev.* **2002**, *31*, 96−107.

(15) Zhang, H.; Paulsen, E. S.; Walker, K. A.; Krakowiak, K. E.; Dearden, D. V. Cucurbit[6]uril Pseudorotaxanes: Distinctive Gas-Phase Dissociation and Reactivity. *J. Am. Chem. Soc.* **2003**, *125*, 9284−9285.

(16) Zhang, H.; Ferrell, T. A.; Asplund, M. C.; Dearden, D. V. Molecular Beads on a Charged Molecular String: α,ω-Alkyldiammonium Complexes of Cucurbit[6]uril in the Gas Phase. *Int. J. Mass Spectrom.* **2007**, *265*, 187−196.

(17) Yang, F.; Jones, C. A.; Selvapalam, N.; Ko, Y. H.; Kim, K.; Dearden, D. V. Binding of α,ω-Alkyldiammonium Ions by Cucurbit-[n]urils in the Gas Phase. *Supramol. Chem.* **2014**, *26*, 684−691.

(18) Meot-Ner, M. The Ionic Hydrogen Bond and Ion Solvation. 1. $NH^+\cdots O$, $NH^+\cdots N$, and $OH^+\cdots O$ Bonds. Correlations with Proton Affinity. Deviations Due to Structural Effects. *J. Am. Chem. Soc.* **1984**, *106*, 1257−1264.

(19) Meot-Ner, M.; Elmore, D. E.; Scheiner, S. Ionic Hydrogen Bond Effects on the Acidities, Basicities, Solvation, Solvent Bridging, and Self-Assembly of Carboxylic Acid Groups. *J. Am. Chem. Soc.* **1999**, *121*, 7625−7635.

(20) Meot-Ner, M.; Sieck, L. W. The Ionic Hydrogen Bond. 1. Sterically Hindered Bonds. Solvation and Clustering of Protonated Amines and Pyridines. *J. Am. Chem. Soc.* **1983**, *105*, 2956−2961.

(21) Meot-Ner, M. The Ionic Hydrogen Bond. 2. Intramolecular and Partial Bonds. Protonation of Polyethers, Crown Ethers, and Diketones. *J. Am. Chem. Soc.* **1983**, *105*, 4906−4911.

(22) Meot-Ner, M. The Ionic Hydrogen Bond. 3. Multiple NH^+-O and $CH^{\delta+}$-O Bonds. Complexes of Ammonium Ions with Polyethers and Crown Ethers. *J. Am. Chem. Soc.* **1983**, *105*, 4912−4915.

(23) Meot-Ner, M. The Ionic Hydrogen Bond. 4. Intramolecular and Multiple Bonds. Protonation and Complexes of Amides and Amino Acid Derivatives. *J. Am. Chem. Soc.* **1984**, *106*, 278−283.

(24) Meot-Ner, M.; Sieck, L. W.; Scheiner, S.; Duan, X. The Ionic Hydrogen Bond. 5. Polydentate and Solvent-Bridged Structures. Complexing of the Proton and the Hydronium Ion by Polyethers. *J. Am. Chem. Soc.* **1994**, *116*, 7848−7856.

(25) Zheng, X.; Aly, N. A.; Zhou, Y.; Dupuis, K. T.; Bilbao, A.; Paurus, V. L.; Orton, D. J.; Wilson, R.; Payne, S. H.; Smith, R. D.; et al. A Structural Examination and Collision Cross Section Database for over 500 Metabolites and Xenobiotics Using Drift Tube Ion Mobility Spectrometry. *Chem. Sci.* **2017**, *8*, 7724−7736.

(26) Ahmed, A.; Cho, Y. J.; No, M.-h.; Koh, J.; Tomczyk, N.; Giles, K.; Yoo, J. S.; Kim, S. Application of the Mason-Schamp Equation and Ion Mobility Mass Spectrometry to Identify Structurally Related Compounds in Crude Oil. *Anal. Chem.* **2011**, *83*, 77−83.

(27) Halgren, T. A. Merck Molecular Force Field. I. Basis, Form, Scope, Parameterization, and Performance of MMFF94. *J. Comput. Chem.* **1996**, *17*, 490−519.

(28) Halgren, T. A. Merck Molecular Force Field. II. MMFF94 Van Der Waals and Electrostatic Parameters for Intermolecular Interactions. *J. Comput. Chem.* **1996**, *17*, 520−552.

(29) Halgren, T. A. Merck Molecular Force Field. III. Molecular Geometries and Vibrational Frequencies for MMFF94. *J. Comput. Chem.* **1996**, *17*, 553−586.

(30) Halgren, T. A.; Nachbar, R. B. Merck Molecular Force Field. IV. Conformational Energies and Geometries for MMFF94. *J. Comput. Chem.* **1996**, *17*, 587−615.

(31) Halgren, T. A. Merck Molecular Force Field. V. Extension of MMFF94 Using Experimental Data, Additional Computational Data, and Empirical Rules. *J. Comput. Chem.* **1996**, *17*, 616−641.

(32) Shrivastav, V.; Nahin, M.; Hogan, C. J.; Larriba-Andaluz, C. Benchmark Comparison for a Multi-Processing Ion Mobility Calculator in the Free Molecular Regime. *J. Am. Soc. Mass Spectrom.* **2017**, *28*, 1540−1551.

(33) Marcus, R. A.; Rice, O. K. The Kinetics of the Recombination of Methyl Radicals and Iodine Atoms. *J. Phys. Colloid Chem.* **1951**, *55*, 894−908.

(34) Robinson, J. P.; Holbrook, K. A. *Unimolecular Reactions*; Wiley: New York, 1972.

(35) Griffin, L.; McAdoo, D. J. The Effect of Ion Size on Rate of Dissociation - RRKM Calculations on Model Large Polypeptide Ions. *J. Am. Soc. Mass Spectrom.* **1993**, *4*, 11−15.
(36) Memboeuf, A.; Nasioudis, A.; Indelicato, S.; Pollreisz, F.; Kuki, Á.; Kéki, S.; van den Brink, O. F.; Vékey, K.; Drahos, L. Size Effect on Fragmentation in Tandem Mass Spectrometry. *Anal. Chem.* **2010**, *82*, 2294−2302.
(37) Muntean, F.; Armentrout, P. B. Modeling Kinetic Shifts and Competition in Threshold Collision-Induced Dissociation. Case Study: N-Butylbenzene Cation Dissociation. *J. Phys. Chem. A* **2003**, *107*, 7413−7422.
(38) Yang, F.; Dearden, D. V. Guanidinium-Capped Cucurbit[7]uril Molecular Cages in the Gas Phase. *Supramol. Chem.* **2011**, *23*, 53−58.

https://doi.org/10.1021/acs.jpca.2c01703
J. Phys. Chem. A 2022, 126, 2950−2958